

Dark matter halo mass density profiles around an accreting supermassive blackhole in the Schrödinger-Newton approach

Chon-Fai Kam*

*Department of Physics and The Hong Kong Institute of Quantum Information Science and Technology,
The Chinese University of Hong Kong, Shatin, New Territories, Hong Kong, China*

Iat-Neng Chan†

*Department of Physics and Chemistry, Faculty of Science and Technology,
University of Macau, Avenida da Universidade, Taipa, Macau, People's Republic of China*

We study how supermassive blackhole accretion affects the mass density profile of a fuzzy dark matter soliton core at the centre of a dark matter halo. The supermassive blackhole at the center of a galaxy was regarded as a point mass. The Schrödinger-Newton equation for the scalar field was solved numerically. We find that the time-dependent perturbation has a significant squeezing effect on the soliton density profile, which both reduces the size of the core and increases the central density.

I. INTRODUCTION

Despite a strong circumstantial evidence for its existence, the exact particle nature of dark matter, which makes up 27% of the Universe's energy density, is still yet unknown and remains one of the biggest mysteries in physics [1]. As dark matter is approximately five times more abundant than baryonic matter such as neutrons and protons, which adds up to less than 5% of the energy density in the universe, it dominates the formation of large-scale structure of the Universe [2], and governs the formation and evolution of galaxies within merging dark matter haloes [3, 4]. Although the nature of dark matter is still unknown, there is overwhelming evidence that dark matter cannot be composed of any particles described by the standard model of particle physics, based on a variety of observations [1]. Among the various possible solutions to the dark matter problem such as neutrinos, light bosons, or modified gravity, the cold dark matter (CDM) model with weakly interacting massive particles (WIMPs) seems the most promising one, since it can successfully simulates the large-scale structure of the Universe [5, 6].

Despite the CDM model being successful in describing the formation of large-scale structure of the Universe, it presents several difficulties to overcome on small scales (\lesssim hundreds of kpc) [7, 8]. The biggest challenge is the so called “cusp-core” (CC) problem [9], where the mass density profile of cold dark matter halos is expected to has a cusp from collisionless N -body simulations of low-mass galaxies, i.e., $\rho \propto r^{-x}$ with $1 \lesssim x \lesssim 1.5$, which deeply contradicts the observed core-like mass density profile, i.e., $\rho \propto r^0$ of dwarf galaxies, irregulars, and low surface brightness galaxies [10–12]. Another challenge is the “missing satellite” (MSP) problem, which refers to a discrepancy between the number of predicted number of halo substructures in collisionless N -body simulations and the observed number of satellite galaxies, i.e., the CDM model predicts that there are around 1000 satellite galaxies in the

Local Group, much higher than the observed number (~ 50) of dwarf galaxies [13, 14]. Due to the discrepancies between the predictions of the CDM model and the actual observations on small scales, and also the lack of direct evidence supporting cold dark matter particles such as the WIMPs with masses of order a few GeV to a few hundred GeV [15], alternative solutions to the dark-matter problem need to be fully exploited.

One possibility is that the galactic dark matter is an ultralight scalar field with negligible self-interactions, which consists of ultralight light scalar bosons with masses of order a few 10^{-22} eV [16, 17]. In this scenario, the ultralight scalar bosons form a Bose-Einstein condensate, in which all particles share one wave function. Such an alternative theoretical model, so called fuzzy cold dark matter (FCDM) model, provides intriguing solutions to the cusp-core problem: the ultralight scalar particles have Compton wavelengths of order a few light years, so that wave-like behaviors are manifest at the galactic scale, and the cusps in the center of the FCDM halos could be avoided due to the Heisenberg uncertainty principle [18, 19]. In this regard, the FCDM model yields a smoother structure compared to the classical collisionless CDM model on scales below a few kpc due to quantum pressure [19]. For example, ultralight scalar bosons with mass of order 10^{-22} eV transform dark matter halo cusps of galaxies into soliton cores of order a few kpc [18, 19]. Beside this the existence of dwarf galaxies in dark matter halos with masses of $\sim 10^9$ times the mass of the Sun in the Local Universe constrain the FCDM model. For smaller boson masses, i.e., $m \lesssim 10^{-24}$ eV, the observed large-scale cosmic structure will be erased; while for larger boson masses, i.e., $m \gtrsim 10^{-20}$ eV, the classical collisionless CDM behavior on all cosmological scales recovers, which makes it difficult to restrict the mass of FCDM particles [18].

Observational evidence indicates that at the center of nearly every large galaxy there is a supermassive black hole with a mass which is million to billion times the mass of the Sun [20, 21]. Hence the study of how dark matter halos evolve under the influence of its central supermassive black hole is a necessary step toward understanding the connection between the galaxies and their surrounding dark-matter environments [22]. Although a fully relativistic analysis of scalar field dark matter evolution around a supermassive blackhole is possi-

* Email: dubussygauss@gmail.com

† Email: inchan@um.edu.mo

ble [23–26], we are here mainly interested in the dark matter halo mass density profile far from the Schwarzschild radius, so that the supermassive blackhole can be represented by a point mass [27]. Such a simplified approach offers the simplest possible theoretical explanation for existing data. As most galactic cores are known to host a massive black hole that is accreting matter and displaying a sufficiently strong luminosity, the impact of blackhole accretion on the dark matter halo mass density profile also merits study. This is the main goal of this work.

II. THE MODEL

To describe the dark matter halo density profiles around an accreting supermassive black hole, we consider a scalar field dark matter model, in which the dark matter are comprised of ultralight fuzzy dark matter (FDM) particles. As the occupation numbers in galactic halos are high, the ultralight fuzzy dark matter can be described by a scalar field $\Psi(\mathbf{r}, t)$ minimally coupled to the gravity, obeying the Schrödinger-Newton equation [28]

$$i\hbar\partial_t\Psi(\mathbf{r}, t) = \left(-\frac{\hbar^2\nabla^2}{2m} + m\Phi(\mathbf{r}, t) + mV(r, t)\right)\Psi(\mathbf{r}, t), \quad (1)$$

where $m \approx 10^{-22}\text{eV}$ is the mass of the fuzzy dark matter particle, $\Phi(\mathbf{r}, t)$ is the self-potential of the wave function which obeys Poisson's equation describing the evolution of the gravitational field in the Newtonian limit

$$\nabla^2\Phi(\mathbf{r}, t) = 4\pi G|\Psi(\mathbf{r}, t)|^2, \quad (2)$$

and $V(r, t)$ is a time-dependent black hole potential given by

$$V(r, t) = -\frac{GM(t)}{r}. \quad (3)$$

Here, $M(t)$ is a time-dependent mass of the black hole, and G is the gravitational constant. According to the standard Shakura-Sunyaev disk (SSD) model for accreting black holes, we assume that the mass of the black hole varies in time as [29]

$$M(t) \equiv M_0 \exp\left(\lambda \frac{1-\epsilon}{\epsilon} \frac{t}{t_E}\right) \equiv M_0 e^{\alpha t}, \quad (4)$$

where $\lambda \equiv L/L_E$ is the *Eddington ratio*, which relates the luminosity L of an accreting super-massive black hole with the *Eddington luminosity* $L_E \equiv 4\pi c G M m_p / \sigma_T$, with σ_T being the Thomson scattering cross-section for the electron, and m_p being the mass of the proton. Here, $\epsilon \approx 0.1$ is the radiative efficiency of accretion, and $t_E \approx 4.5 \times 10^7 \text{yrs}$ is the Salpeter time scale — an e-folding time-scale for super-massive black hole growth. As the Poisson equation for the self-potential $\Phi(\mathbf{r}, t)$ is solved by the integral

$$\Phi(\mathbf{r}, t) = -G \int \frac{|\Psi(\mathbf{r}', t)|^2}{|\mathbf{r} - \mathbf{r}'|} d^3 r', \quad (5)$$

the scalar field $\Psi(\mathbf{r}, t)$ obeys the following differential-integral equation

$$i\hbar\partial_t\Psi(\mathbf{r}, t) = \left(-\frac{\hbar^2\nabla^2}{2m} - Gm \int \frac{|\Psi(\mathbf{r}', t)|^2}{|\mathbf{r} - \mathbf{r}'|} d^3 r' - Gm \frac{M(t)}{r}\right)\Psi(\mathbf{r}, t). \quad (6)$$

For spherically symmetric solutions, one obtains a 1+1 dimensional differential integral equation which governs the spherically symmetric solutions of the scalar field

$$\begin{aligned} i\hbar\partial_t\Psi(r, t) &= -\frac{\hbar^2}{2mr} \frac{\partial^2}{\partial r^2}(r\Psi(r, t)) - Gm \left(\frac{4\pi}{r} \int_0^r |\Psi(r', t)|^2 r'^2 dr' \right. \\ &\quad \left. + 4\pi \int_r^\infty |\Psi(r', t)|^2 r' dr' + \frac{M_0 e^{\alpha t}}{r}\right) \Psi(r, t) \\ &\equiv \hat{H}(r, t)\Psi(r, t). \end{aligned} \quad (7)$$

III. THE NUMERICAL METHOD

We now use the Crank-Nicolson scheme to solve the above 1+1 dimensional differential integral equation. To do so, we define the spatial and temporal grid sizes as Δr and Δt respectively, and use the index notation $\Psi_k^n(r, t) \equiv \Psi(k\Delta r, n\Delta t)$. Then, we can write Eq. (7) in the Cayley form as [30, 31]

$$\exp\left(\frac{i\Delta t \hat{H}}{2\hbar}\right) \Psi_k^{n+1} = \exp\left(-\frac{i\Delta t \hat{H}}{2\hbar}\right) \Psi_k^n. \quad (8)$$

After linearization, it can be written as

$$\Psi_k^{n+1} = (\hat{Q}^{-1} - 1)\Psi_k^n, \quad \hat{Q} \equiv \frac{1}{2} \left(1 + \frac{i\Delta t}{2\hbar} \hat{H}\right). \quad (9)$$

Or equivalently, a system of linear equations

$$\Psi_k^{n+1} = \chi^n - \Psi_k^n, \quad \chi^n \equiv \hat{Q}^{-1} \Psi_k^n. \quad (10)$$

Here, the radial part of the Laplacian has the form

$$\nabla^2 \equiv \frac{\partial^2}{\partial r^2} + \frac{2}{r} \frac{\partial}{\partial r} \quad \text{for } r > 0, \quad (11a)$$

$$\nabla^2 = 3 \frac{\partial^2}{\partial r^2} \quad \text{for } r = 0, \quad (11b)$$

where the finite difference discretization scheme for the radial part of the Laplacian is (see Appendix B)

$$\nabla^2 \Psi_k^n = \frac{1}{(\Delta r)^2} \left(\frac{k+1}{k} \Psi_{k+1}^n - 2\Psi_k^n + \frac{k-1}{k} \Psi_{k-1}^n \right) \quad \text{for } k > 0, \quad (12a)$$

$$\nabla^2 \Psi_k^n = \frac{6}{(\Delta r)^2} (\Psi_1^n - \Psi_0^n) \quad \text{for } k = 0. \quad (12b)$$

Besides, the discretization of the self-potential and the black hole potential have the form

$$\Phi_k^n \approx -4\pi G(\Delta r)^2 \left(\frac{1}{k} \sum_{i=0}^{k-1} |\Psi_i^n|^2 i^2 + \sum_{i=k}^{N-1} |\Psi_i^n|^2 i \right) \equiv -4\pi G(\Delta r)^2 f_k^n, \quad (13a)$$

$$V_k^n = -GM_0 \frac{\exp(\alpha n \Delta t)}{k(\Delta r)} \equiv -GM_0 g_k^n. \quad (13b)$$

Away from the origin and the point before spatial infinity of the spatial grid, i.e., $k \neq 0, N-1$, one obtains the finite difference equations

$$\hat{Q}\chi_k^n \equiv a_k \chi_{k-1}^n + b_k \chi_k^n + c_k \chi_{k+1}^n, \quad (14a)$$

$$a_k \equiv \beta \frac{k-1}{k}, \quad b_k \equiv \frac{1}{2} - 2\beta + \gamma f_k^n + \delta g_k^n, \quad c_k \equiv \beta \frac{k+1}{k}, \quad (14b)$$

$$\beta \equiv -\frac{i\hbar}{8m} \frac{\Delta t}{(\Delta r)^2}, \quad \gamma \equiv \frac{-i\pi G m(\Delta r)^2 \Delta t}{\hbar}, \quad \delta \equiv \frac{-iGM_0 m \Delta t}{4\hbar}. \quad (14c)$$

Similarly, at the point directly before spatial infinity of the spatial grid, i.e., $k = N-1$, one obtains the finite difference equation $\hat{Q}\chi_{N-1}^n = a_{N-1}\chi_{N-2}^n + b_{N-1}\chi_{N-1}^n$, where the coefficients a_{N-1} and b_{N-1} are given by Eqs. (14b) - (14c) by substituting k for $N-1$. Finally, at the origin, i.e., $k = 0$, one obtains the finite difference equation $\hat{Q}\chi_0^n \equiv b_0\chi_0^n + c_0\chi_0^n$, where $b_0 \equiv \frac{1}{2} - 6\beta + \gamma f_0^n + \delta g_0^n$, and $c_0 \equiv 6\beta$. Denoting $\tau \equiv t/t_E$, one obtains the dimensionless finite difference equation at the $(n+1)$ th time step, $\tilde{\Psi}_k^{n+1} = (\hat{Q}^{-1} - 1)\tilde{\Psi}_k^n$, where

$$\hat{Q}\tilde{\Psi}_k^n = \tilde{a}_k \tilde{\Psi}_{k-1}^n + \tilde{b}_k \tilde{\Psi}_k^n + \tilde{c}_k \tilde{\Psi}_{k+1}^n, \quad \tilde{\Psi}_k^n \equiv \sqrt{4\pi G} t_E \Psi_k^n, \quad (15a)$$

$$\tilde{a}_k \equiv \tilde{\beta} \frac{k-1}{k}, \quad \tilde{b}_k \equiv \frac{1}{2} - 2\tilde{\beta} + \tilde{\gamma} \tilde{f}_k^n + \tilde{\delta} \tilde{g}_k^n, \quad \tilde{c}_k \equiv \tilde{\beta} \frac{k+1}{k}, \quad (15b)$$

$$\tilde{\alpha} \equiv \alpha t_E, \quad \tilde{\beta} \equiv \frac{-i\Delta\tau}{8(\Delta u)^2}, \quad \tilde{\gamma} \equiv \frac{-i(\Delta u)^2 \Delta\tau}{4}, \quad \tilde{\delta} \equiv \frac{-i\lambda \Delta\tau}{4}. \quad (15c)$$

Hence, \hat{Q} can be represented as a sparse N by N matrix in a tridiagonal form

$$\hat{Q} \equiv \begin{pmatrix} b_0 & c_0 & 0 & 0 & \cdots & 0 \\ a_1 & b_1 & c_1 & 0 & \cdots & 0 \\ 0 & a_2 & b_2 & c_2 & \cdots & 0 \\ \vdots & \vdots & \vdots & \ddots & \vdots & \vdots \\ 0 & 0 & \cdots & a_{N-2} & b_{N-2} & c_{N-2} \\ 0 & 0 & \cdots & 0 & a_{N-1} & b_{N-1} \end{pmatrix}. \quad (16)$$

Notice that only the coefficients b_k are time-dependent, since they contain a sum over the self-potential and the time-dependent black hole potential. Here, the initial condition for the scalar field $\Psi(r, t)$ is fixed by setting $\Psi(r, 0) = \phi(r)$, where $\phi(r)$ is the steady-state spherical solution for $\alpha = 0$, which corresponds to a time independent black hole potential with a mass $M(t) \equiv M_0$.

IV. THE STEADY-STATE SPHERICAL SOLUTION

The steady-state spherical solution $\phi(r)$ can be solved by the ansatz $\Psi(r, t) = e^{-iEt/\hbar} \phi(r)$, so that the Schrodinger-Poisson

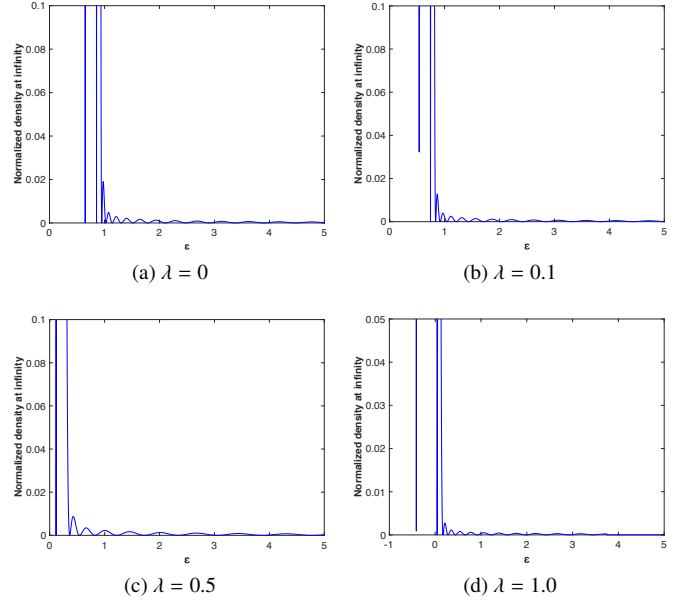


FIG. 1. Schematic of the asymptotic normalized densities $\tilde{\phi}(u)^2$ for $u \rightarrow \infty$ as functions of the parameter ϵ for different λ values, where $\lambda \equiv GM_0 m / (\hbar c)$ is the dimensionless mass of the black hole. Here, we fixed the dimensionless distance u to 15 when evaluating the asymptotic normalized densities $\tilde{\phi}(u)^2$.

equation for a time-independent black hole potential becomes

$$E\phi(r) = \left(-\frac{\hbar^2}{2m} \nabla^2 + m\Phi(r) + mV(r) \right) \phi(r), \quad (17a)$$

$$\nabla^2 \Phi(r) = 4\pi G |\phi(r)|^2. \quad (17b)$$

Or equivalently

$$\frac{\hbar^2}{2m} \frac{d^2}{dr^2} (r\phi(r)) = (rm\Phi(r) - rE - GmM_0) \phi(r), \quad (18a)$$

$$\frac{d^2}{dr^2} (r\Phi(r)) = 4\pi G r \phi(r)^2, \quad (18b)$$

which are subjected to the initial conditions $\phi(0) = 1$, $\phi'(0) = \Phi(0) = \Phi'(0) = 0$ and the boundary condition $\phi(\infty) = 0$. We use the shooting method to solve the above set of differential equations, which starts by a trial solution at $r = 0$, and tries to reach the asymptotic boundary condition at $r = \infty$. To simplify numerical computation, one may introduce a set of dimension-less variables via

$$u \equiv \frac{r}{L_0}, \quad \tilde{\Phi} \equiv \frac{\Phi}{c^2}, \quad \epsilon \equiv \frac{E}{mc^2}, \quad (19)$$

so that the renormalized time-independent coupled SP equations becomes

$$\frac{d^2}{du^2} (u\tilde{\phi}) = 2u \left(\tilde{\Phi} - \epsilon - \frac{\lambda}{u} \right) \tilde{\phi}, \quad (20a)$$

$$\frac{d^2}{du^2} (u\tilde{\Phi}) = u\tilde{\phi}^2, \quad (20b)$$

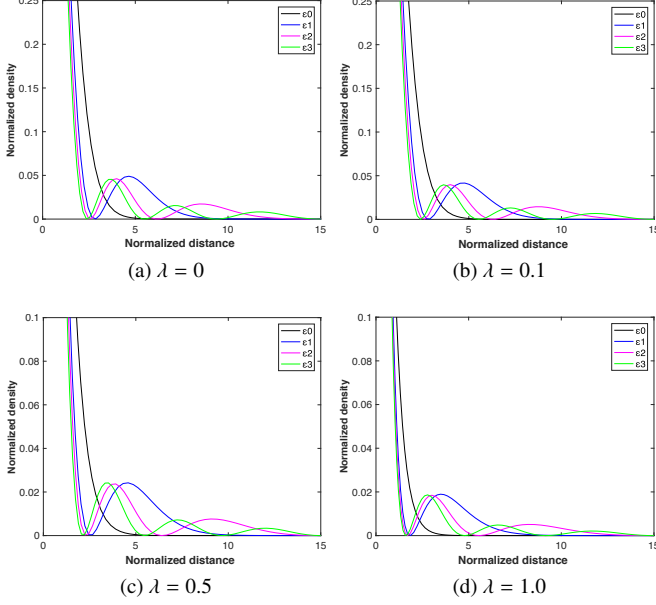


FIG. 2. Schematic of the normalized densities $\tilde{\phi}_n^2 \equiv 4\pi G\hbar^2 \phi_n^2 / (m^2 c^4)$ as functions of the normalized distance $u \equiv mcr/\hbar$ for different λ values, where n is an integer which labels the discrete eigenvalues ϵ_n , and $\lambda \equiv GM_0 m / (\hbar c)$ is the dimensionless mass of the black hole. Here, we only plot the normalized densities for the first four eigenvalues.

λ	ϵ_0	ϵ_1	ϵ_2	ϵ_3
0	0.649599900660242	0.855382257832184	0.950376	1.027724
0.1	0.537515694614713	0.742953148283380	0.836921	0.918315
0.5	0.116385322639802	0.360002326932728	0.459582	0.560518
1.0	-0.411778217857106	0.043028169337089	0.171107	0.281542

TABLE I. Table of the four smallest eigenvalues ϵ_n which obey the asymptotic boundary condition $\tilde{\phi}(\infty) = 0$ for different values of λ .

where $L_0 \equiv \hbar/(mc)$, $\lambda \equiv GM_0 m / (\hbar c)$, and $\tilde{\phi} \equiv \sqrt{4\pi G} L_0 \phi / c$. As an example, for $m \approx 10^{-22}$ eV, one obtains $L_0 \approx 0.1380$ m, $\lambda \approx 5.3832 \times 10^{-27} M_0$, and $\tilde{\phi} \approx 1.3326 \times 10^{-14} \phi$. The above coupled SP equations can be written as a system of first-order ordinary differential equation as

$$y_1' = y_2, \quad (21a)$$

$$y_2' = -\frac{2}{u} y_2 + 2 \left(y_3 - \epsilon - \frac{\lambda}{u} \right) y_1, \quad (21b)$$

$$y_3' = y_4, \quad (21c)$$

$$y_4' = -\frac{2}{u} y_4 + y_1^2, \quad (21d)$$

where $y_1 \equiv \tilde{\phi}$, $y_3 \equiv \tilde{\Phi}$. One may also simplify the the coupled SP equations by introducing $y_1 \equiv u\tilde{\phi}$ and $y_3 \equiv u\tilde{\Phi} - \lambda$, which obey the following set of coupled differential equations

$$y_1'' = 2 \left(\frac{y_3}{u} - \epsilon \right) y_1, \quad (22a)$$

$$y_3'' = \frac{1}{u} y_1^2, \quad (22b)$$

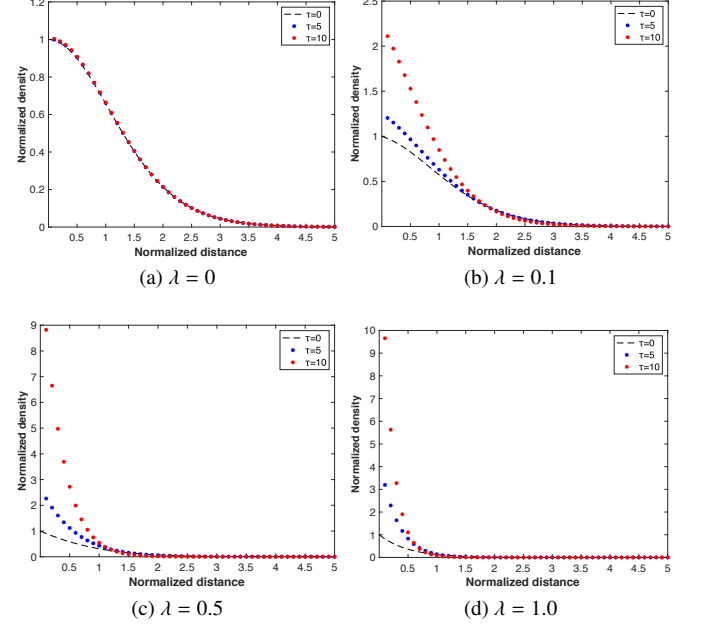


FIG. 3. Schematic of the normalized densities $|\tilde{\Psi}(u, \tau)|^2 \equiv 4\pi G\hbar^2 / (m^2 c^4) |\Psi(r, t)|^2$ as functions of radical distance and time in the dimensionless units for an initial 0-node solution (ground state) for $\lambda \equiv GM_0 m / (\hbar c) = 0, 0.1, 0.5$ and 1.0 respectively. Here, we fix the value of $\alpha = 0.1$ for different values of λ .

where the initial conditions are $y_1(0) = 0$, $y_1'(0) = 1$, $y_3(0) = -\lambda$, and $y_3'(0) = 0$, and the asymptotic boundary condition at infinity is $\lim_{u \rightarrow \infty} u^{-1} y_1 = 0$. Eqs. (22a) - (22b) can be written as a system of first-order ordinary differential equations as

$$y_1' = y_2, \quad (23a)$$

$$y_2' = 2 \left(\frac{y_3}{u} - \epsilon \right) y_1, \quad (23b)$$

$$y_3' = y_4, \quad (23c)$$

$$y_4' = \frac{1}{u} y_1^2. \quad (23d)$$

where the initial conditions are $y_1(0) = 0$, $y_2(0) = 1$, $y_3(0) = -\lambda$, and $y_4(0) = 0$.

V. RESTRICTIONS ON FUZZY DARK MATTER PARTICLE MASS

A. The mass-radius relation for the soliton/ boson star

For an intuiting understanding of nonlinear, bound objects like solitons or boson stars, one can start with the analysis of different energy scales. In particular, solitons are those compact objects in which quantum pressure balances gravitational potential energy. i.e.,

$$\frac{GM_s}{R_s} \propto \frac{1}{2m^2} \frac{\nabla^2 \sqrt{\rho}}{\sqrt{\rho}} \propto \frac{1}{m^2 R_s^2}, \quad (24)$$

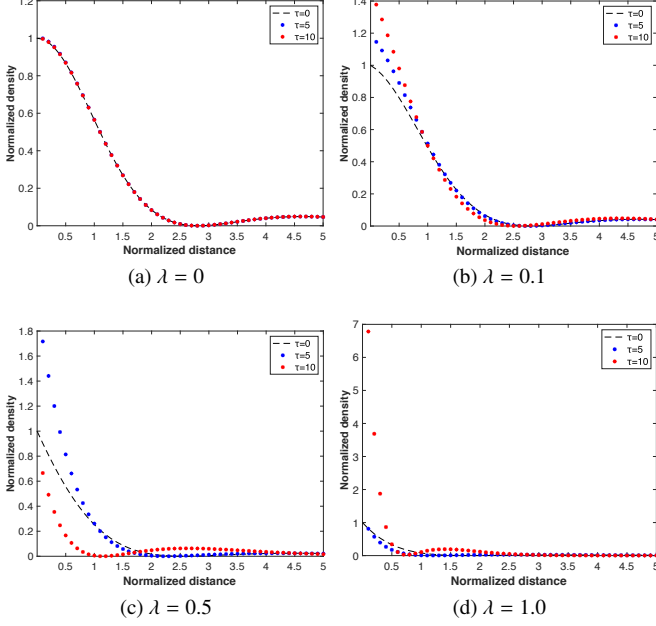


FIG. 4. Schematic of the normalized densities $|\tilde{\Psi}(u, \tau)|^2 \equiv 4\pi G\hbar^2/(m^2 c^4)|\Psi(r, t)|^2$ as functions of radical distance and time in the dimensionless units for an initial 1-node solution (lowest excited state) for $\lambda \equiv GM_0 m/(\hbar c) = 0, 0.1, 0.5$ and 1.0 respectively. Here, we fix the value of $\alpha = 0.1$ for different values of λ .

where $\rho \equiv m|\phi|^2$ is the mass density, R_s is the radius of the soliton, and M_s is the total mass of the soliton given by [27]

$$M_s \equiv \int_0^\infty |\phi|^2 4\pi r^2 dr = \frac{\hbar c}{Gm} \int_0^\infty \tilde{\phi}^2 u^2 du \equiv \frac{\hbar c \tilde{M}_s}{Gm}, \quad (25)$$

where $u \equiv r/L_0$, $L_0 \equiv \hbar/(mc)$, $\tilde{\phi} \equiv \sqrt{4\pi G} L_0 \phi/c$, and \tilde{M}_s is the normalized total mass of the soliton. The constant $\hbar c/(Gm)$ sets the mass of the soliton and is given by

$$\frac{\hbar c}{Gm} \approx 1.336 \times 10^{12} M_\odot \left(\frac{10^{-22} \text{eV}}{m} \right). \quad (26)$$

One may introduce the dimensionless ratio of the black hole mass to the soliton mass, $\eta \equiv \lambda/\tilde{M}_s = M_0/M_s$, where M_0 is the mass of the supermassive black hole, and λ sets the dimensionless mass of the black hole. Clearly, the mass ratio η is invariant under scaling, and is the main factor which determines the density profile of the soliton.

From Eq. (24), one deduces that the total mass of a soliton is inversely proportional to its core size, i.e., [32]

$$M_s R_s \propto \frac{1}{Gm^2} \propto 2.2 \times 100 \text{pc} \times 10^9 M_\odot \left(\frac{10^{-22} \text{eV}}{m} \right)^2. \quad (27)$$

Using the data $1 \text{pc} = 3.085677581 \times 10^{16} \text{m}$, one obtains the mass-radius relation for a soliton in the dimensionless unit

$$\tilde{M}_s U_s = 2.57436836743. \quad (28)$$

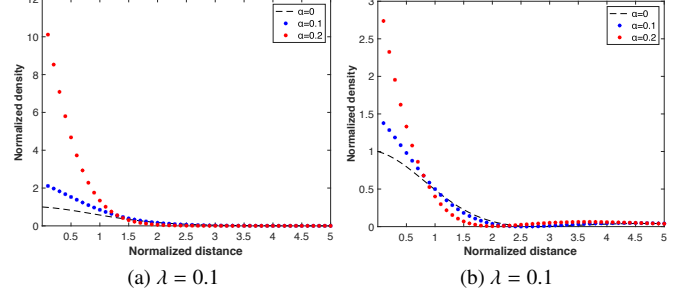


FIG. 5. Schematic of the normalized densities $|\tilde{\Psi}(u, \tau)|^2 \equiv 4\pi G\hbar^2/(m^2 c^4)|\Psi(r, t)|^2$ as functions of radical distance and time in the dimensionless units for $\alpha = 0, 0.1$ and 0.2 respectively. In the left panel we plot the normalized densities for an initial 0-node solution (ground state), while in the right panel we plot the normalized densities for an initial 1-node solution (lowest excited state). Here, we fix the value of $\lambda = 0.1$ for different values of α .

B. Soliton condensation: the relationship between the soliton mass and the halo mass

On the large scale of the Universe, it was first pointed out by Schive et al. [34, 35] from the cosmological simulations that, virialized halos tend to have a core with a soliton mass that scales with the halo mass as:

$$M_s \propto a^{-1/2} M_h^{1/3}, \quad (29)$$

where a is the cosmic scale factor, M_s is the soliton mass, and M_h is the dark matter halo mass. Employing the scaling relation at the present age of the Universe ($a = 1$), one obtains

$$M_s \approx 1.25 \times 10^9 M_\odot \left(\frac{M_h}{10^{12} M_\odot} \right)^{1/3} \left(\frac{10^{-22} \text{eV}}{m} \right). \quad (30)$$

As a remark, a dark matter halo is said to be virialized when it has reached an equilibrium between the kinetic and potential energy, and obeys the virial theorem [32]. The virial radius of a dark matter halo is the radius that which the density of the halo equals 200 times the critical density of the Universe. The mass contained inside the virial radius is regarded as the total mass of the dark matter halo.

C. The relationship between the soliton mass and the FDM particle mass

The restriction of the range of dark matter soliton mass mainly comes from the cosmological setting. In order that the soliton does not collapse directly to a black hole, there is an upper limit of the soliton mass [32]: $GM/R \lesssim 1$. Substitution in the mass-radius relation for the soliton yields the maximum soliton mass M_2 [33]

$$M_2 \propto \frac{1}{Gm} \propto 8.46 \times 10^{11} M_\odot \left(\frac{m}{10^{-22} \text{eV}} \right). \quad (31)$$

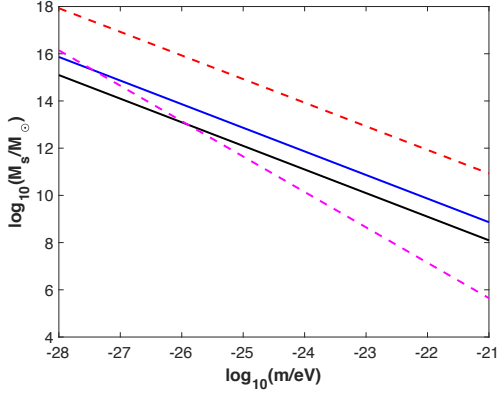


FIG. 6. The log-log plot of the soliton mass M_s against the fuzzy dark matter mass m . The total mass of the soliton at the center of the Milky Way and M87 are shown with dark and blue solid curves respectively. The soliton mass is obtained from the relationship between the soliton mass and the mass of halos where the galaxies reside. The upper and the lower bounds of the dark matter soliton mass are shown by red and magenta broken lines respectively.

Similarly, there is a lower limit of the soliton mass. The soliton ceases to exist if the central density is lower than 200 times the critical density of the Universe, as we have remarked above. Numerically, the minimum soliton mass M_1 is [33]

$$M_1 \propto 1.40 \times 10^7 M_\odot \left(\frac{m}{10^{-22} \text{eV}} \right)^{-3/2}. \quad (32)$$

Finally, using the following data

$$\frac{GM_\odot}{c^2} = 14.7662563825 \times 10^8 \mu\text{m}, \quad (33a)$$

$$\hbar c = 0.1973269804 \text{eV} \times \mu\text{m}, \quad (33b)$$

one readily obtains from Eq. (25) the numerical relationship between the soliton mass and the FDM particle mass

$$M_s/M_\odot = 1.336337765 \times 10^{-x-10} \times \tilde{M}_s, \quad (34)$$

where $x \equiv \log_{10}(m/\text{eV})$, and \tilde{M}_s is the normalized total mass of the soliton.

VI. THE RESULT

From Figs. 1 and 2, one can see that, for a given dimensionless black hole mass λ , there are a unique set of discrete eigenvalues ϵ_n which obey the asymptotic boundary condition $\phi(\infty) = 0$. In the dimensionless unit, the eigenvalues ϵ_n and the associated eigenfunctions $\tilde{\phi}_n$ are labeled by the number of nodes of $\tilde{\phi}(u)$ as functions of the normalized distance $u \equiv mcr/\hbar$. The 0-node solution in the fuzzy dark matter theory is regarded as the soliton, or boson star. In other words, the dimensionless black hole mass determines the density profile of the soliton.

In Table. I, we list the first few lowest discrete eigenvalues of the nonlinear Schrödinger-Newton equation. Unlike its linear counterpart, the asymptotic boundary condition $\phi(\infty) = 0$

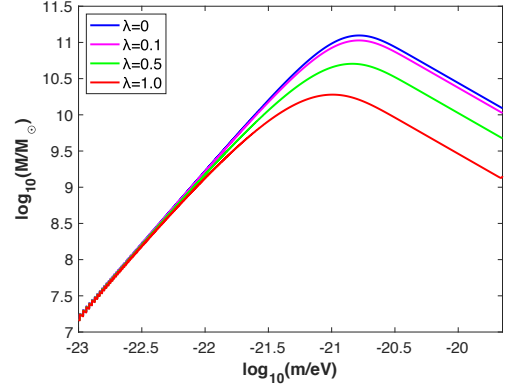


FIG. 7. The log-log plot of the enclosed soliton mass M within a radius of $r \approx 0.01 \text{pc}$ near the central supermassive black hole against the fuzzy dark matter mass m . Here, the dimensionless mass of the supermassive black hole is chosen to be 0, 0.1, 0.5 and 1.0 respectively.

cannot be truly satisfied as it requires an infinite accuracy of the nonlinear eigenvalues. To ensure sufficient accuracy, we retain 16 digits in the computation of the lowest eigenvalues.

In Fig. 3, we plot the FDM soliton mass density profile with respect to the radial distance in the dimensionless unit for an initial 0-node solution. The results show that when the black hole is accreting at a fixed accretion rate (e.g., $\alpha = 0.1$), the dark matter soliton density profile for an initial 0-node solution is squeezed near the central supermassive black hole. For a fixed accretion rate, the squeezing effects for larger black holes are more significant than those for smaller black holes. In Fig. 4, the schematic of the FDM soliton mass density profile for an initial 1-node solution also shows significant squeezing effects surrounding the central black hole.

In Fig. 5, we compare the FDM soliton-like mass density profiles with a fixed dimensionless black hole mass $\lambda = 0.1$ for different accretion rates, i.e., $\alpha = 0, 0.1$ and 0.2 . The result shows that the squeezing effects are more significant when the accretion rate for the central supermassive increases, and is weakened for an initial 1-node solution compared to an initial 0-node FDM soliton.

In Fig. 6, we see that for a fuzzy dark matter particle with a mass $m \lesssim 10^{-26} \text{eV}$, the total mass of the FDM soliton at the center of Milky Way already fails below the lower bound. Hence, the mass of FDM particle has to be $m \gtrsim 10^{-26} \text{eV}$.

In Fig. 7, we compare the mass profile of different solitons near the galactic central supermassive black hole ($M_0 \propto 10^5 \sim 10^{10} M_\odot$) with dimensionless masses $\lambda \equiv GM_0 m / (\hbar c)$ ranging from 0 to 1, where M_0 is the mass of the supermassive black hole. The mass profile is mainly unaffected by the FDM particle mass when $m \lesssim 10^{-22.5} \text{eV}$, and is significantly modulated by the FDM particle mass when $m \gtrsim 10^{-22.5} \text{eV}$. Surrounding a supermassive black hole, the mass of enclosed soliton can be lowered by two orders of magnitude, when the black hole mass is comparable to the total mass of the soliton.

VII. CONCLUSION

We numerically computed the mass density profiles of the soliton cores in the center of fuzzy dark matter halos by solving the Schrödinger-Newton equation with the presence of a time-dependent point mass perturber which represents the supermassive blackhole accretion at the center of galaxy. We showed that there is a significant squeezing effects on the density profile in both the core size and the central density.

Here our computation for the density profiles is non-relativistic. In future works, we may perform a fully relativistic analysis of scalar field dark matter evolution around an accreting supermassive blackhole, as well as self-consistent time-dependent simulations of the blackhole-soliton-halo system.

Appendix A: Derivation of the 1+1 dimensional differential integral equation for spherically symmetric solutions

For spherically symmetric solutions, one may use the Laplace expansion of the inverse distance between the two points \mathbf{r} and \mathbf{r}'

$$\frac{1}{|\mathbf{r} - \mathbf{r}'|} = \sum_{l=0}^{\infty} \frac{4\pi}{2l+1} \frac{r_{<}^l}{r_{>}^{l+1}} Y_l^{-m}(\theta, \phi) Y_l^m(\theta', \phi'), \quad (\text{A1})$$

where $r_{<} = \min(r, r')$, $r_{>} = \max(r, r')$, and $Y_l^m(\theta, \phi)$ is a normalized spherical harmonic function. Then, an integration of the inverse distance between the two points \mathbf{r} and \mathbf{r}' weighted by the density $|\Psi(r', t)|^2$ becomes

$$\begin{aligned} & \sum_{l=0}^{\infty} \frac{4\pi}{2l+1} \int_0^{\infty} |\Psi(r', t)|^2 r'^2 dr' \frac{r_{<}^l}{r_{>}^{l+1}} Y_l^{-m}(\theta, \phi) \int Y_l^m(\theta', \phi') d\Omega' \\ &= \sum_{l=0}^{\infty} \frac{4\pi}{2l+1} \int_0^{\infty} |\Psi(r', t)|^2 r'^2 dr' \frac{r_{<}^l}{r_{>}^{l+1}} Y_l^{-m}(\theta, \phi) \sqrt{4\pi} \delta_{l,0} \delta_{m,0} \\ &= \frac{4\pi}{r} \int_0^r |\Psi(r', t)|^2 r'^2 dr' + 4\pi \int_r^{\infty} |\Psi(r', t)|^2 r' dr', \end{aligned} \quad (\text{A2})$$

where $d\Omega' \equiv \sin \theta' d\theta' d\phi'$ is the differential solid angle in the direction (θ', ϕ') . Using the composite trapezoidal rule, one may discretize the first integral along the radial spatial direction as

$$\frac{4\pi(\Delta r)^2}{k} \left(\sum_{j=1}^{k-1} |\Psi_j(t)|^2 j^2 + \frac{k^2}{2} |\Psi_k(t)|^2 \right) \text{ for } k > 1, \quad (\text{A3a})$$

$$4\pi(\Delta r)^2 \cdot \frac{1}{2} |\Psi_1(t)|^2 \text{ for } k = 1, \quad (\text{A3b})$$

where $r \equiv k\Delta r$ and $\Psi_j(t) \equiv \Psi(j\Delta r, t)$. Similarly, one may discretize the second integral along the radial spatial direction

as

$$4\pi(\Delta r)^2 \left(\frac{k}{2} |\Psi_k(t)|^2 + \sum_{j=k+1}^{N-1} |\Psi_j(t)|^2 j + \frac{N}{2} |\Psi_N(t)|^2 \right) \text{ for } k < N-1, \quad (\text{A4})$$

$$4\pi(\Delta r)^2 \left(\frac{N-1}{2} |\Psi_{N-1}(t)|^2 + \frac{N}{2} |\Psi_N(t)|^2 \right) \text{ for } k = N-1, \quad (\text{A5})$$

where $r_{\max} \equiv N\Delta r$ for a large positive integer N represents the spatial infinity. Hence, for $0 < k < N-1$, the discretization of the self-potential along the radial spatial direction has the form

$$\begin{aligned} \Phi_k(t) &= -4\pi G(\Delta r)^2 \left(\frac{1}{k} \sum_{j=1}^k |\Psi_j(t)|^2 j^2 \right. \\ &\quad \left. + \sum_{j=k+1}^{N-1} |\Psi_j(t)|^2 j + \frac{N}{2} |\Psi_N(t)|^2 \right), \end{aligned} \quad (\text{A6})$$

where $\Phi_k(t) \equiv \Phi(k\Delta r, t)$ and we used the boundary condition $\Psi_N(t) = 0$ at the spatial infinity. In particular, for $k = N-1$, the discretization of the self-potential in the radial direction has the form

$$\Phi_1(t) = -4\pi G(\Delta r)^2 \left(\frac{1}{k} \sum_{j=1}^{N-1} |\Psi_j(t)|^2 j + \frac{N}{2} |\Psi_N(t)|^2 \right). \quad (\text{A7})$$

For a non-uniform partition of $[0, r_k]$ such that $0 = r_0 < r_1 < \dots < r_{k-1} < r_k$, the trapezoidal rule yields the discretization of the first integral along the spatial direction

$$\frac{4\pi}{r_k} \left[\frac{1}{2} \sum_{j=1}^k (|\Psi_{j-1}(t)|^2 r_{j-1}^2 + |\Psi_j(t)|^2 r_j^2) \Delta r_j \right], \quad (\text{A8})$$

where $\Delta r_j \equiv r_j - r_{j-1}$. Similarly, for a non-uniform partition of $[r_k, r_{\max}]$ such that $r_k < r_{k+1} < \dots < r_{N-1} < r_N = r_{\max}$, the trapezoidal rule yields the discretization of the second integral along the spatial direction

$$4\pi \left[\frac{1}{2} \sum_{j=k+1}^N (|\Psi_{j-1}(t)|^2 r_{j-1} + |\Psi_j(t)|^2 r_j) \Delta r_j \right]. \quad (\text{A9})$$

Using the central difference formula, the discretization of the second order derivative of $\Psi(r, t)$ with respect to r at r_k reads

$$\begin{aligned} \left. \frac{\partial^2 \Psi(r, t)}{\partial r^2} \right|_{r=r_k} &= \frac{\Psi'(r_{k+1/2}, t) - \Psi'(r_{k-1/2}, t)}{r_{k+1/2} - r_{k-1/2}} \\ &= \frac{2}{\Delta r_{k+1} + \Delta r_k} \left(\frac{\Psi(r_{k+1}, t) - \Psi(r_k, t)}{\Delta r_{k+1}} - \frac{\Psi(r_k, t) - \Psi(r_{k-1}, t)}{\Delta r_k} \right) \\ &= \frac{2\Psi_{k+1}(t)}{(\Delta r_{k+1} + \Delta r_k)\Delta r_{k+1}} - \frac{2\Psi_k(t)}{\Delta r_{k+1}\Delta r_k} + \frac{2\Psi_{k-1}(t)}{(\Delta r_{k+1} + \Delta r_k)\Delta r_k}. \end{aligned} \quad (\text{A10})$$

Similarly, the discretization of the first order derivative of $\Psi(r, t)$ with respect to r at r_k reads

$$\left. \frac{\partial \Psi(r, t)}{\partial r} \right|_{r=r_k} = \frac{\Psi_{k+1}(t) - \Psi_{k-1}(t)}{\Delta r_{k+1} + \Delta r_k}. \quad (\text{A11})$$

Hence, the finite difference formula for the radial part of the Laplacian reads

$$\nabla^2 \Psi(r, t) \Big|_{r=r_k} \equiv \left(\frac{\partial^2}{\partial r^2} + \frac{2}{r} \frac{\partial}{\partial r} \right) \Big|_{r=r_k} = \frac{2\Psi_{k+1}(t)}{(\Delta r_{k+1} + \Delta r_k) \Delta r_{k+1}} \frac{r_{k+1}}{r_k} - \frac{2\Psi_k(t)}{\Delta r_{k+1} \Delta r_k} + \frac{2\Psi_{k-1}(t)}{(\Delta r_{k+1} + \Delta r_k) \Delta r_k} \frac{r_{k-1}}{r_k}. \quad (\text{A12})$$

Appendix B: Boundary conditions for the scalar field at $r \rightarrow 0$

In this work, the boundary conditions for the scalar field $\Psi(r, t)$ are given by

$$\partial_r \Psi(0, t) = 0 \text{ and } \Psi(\infty, t) = 0. \quad (\text{B1})$$

For the radical part of the Laplacian, one obtains

$$\lim_{r \rightarrow 0} \nabla^2 \Psi(r, t) \equiv \lim_{r \rightarrow 0} \left(\frac{\partial^2}{\partial r^2} + \frac{2}{r} \frac{\partial}{\partial r} \right) \Psi(r, t) = 3 \frac{\partial^2 \Psi}{\partial r^2}(r, t), \quad (\text{B2})$$

where we have used the L'Hospital's Rule to determine the indeterminate form of $0/0$

$$\lim_{r \rightarrow 0} \frac{1}{r} \frac{\partial \Psi(r, t)}{\partial r} = \frac{\partial^2 \Psi(r, t)}{\partial r^2}. \quad (\text{B3})$$

The finite difference discretization of the boundary condition at $r \rightarrow 0$ has the form

$$\lim_{r \rightarrow 0} \frac{\partial \Psi}{\partial r}(r, t) \approx \frac{\Psi_1^n - \Psi_{-1}^n}{2\Delta r} = 0, \quad (\text{B4})$$

which yields the boundary condition $\Psi_1^n = \Psi_{-1}^n$ at arbitrary time steps n . Hence, the finite difference discretization of the radical part of the Laplacian has the form

$$\lim_{r \rightarrow 0} \nabla^2 \Psi(r, t) = \frac{3}{(\Delta r)^2} (\Psi_1^n - 2\Psi_0^n + \Psi_{-1}^n) = \frac{6}{(\Delta r)^2} (\Psi_1^n - \Psi_0^n). \quad (\text{B5})$$

-
- [1] G. Bertone and T. M. P. Tait, *Nature* **562**, 51 (2018).
 - [2] C. S. Frenk and S. D. M. White, *Ann. Phys. (Berl.)* **524**, 507 (2012).
 - [3] M. Vogelsberger, F. Marinacci, P. Torrey, and E. Puchwein, *Nat. Rev. Phys.* **2**, 42 (2020).
 - [4] I. de Martino, S. S. Chakrabarty, V. Cesare, A. Gallo, L. Ostorero, and A. Diaferio, *Universe* **6**, 107 (2020).
 - [5] M. Davis, G. Efstathiou, C. S. Frenk, and S. D. M. White, *Astrophys. J.* **292**, 371 (1985).
 - [6] V. Springel, S. D. M. White, A. Jenkins, C. S. Frenk, N. Yoshida, L. Gao, J. Navarro, R. Thacker, D. Croton, J. Helly, J. A. Peacock, S. Cole, P. Thomas, H. Couchman, A. Evrard, J. Colberg, and F. Pearce, *Nature* **435**, 629 (2005).
 - [7] D. H. Weinberg, J. S. Bullock, F. Governato, R. K. de Naray, and A. H. Peter, *Proc. Natl. Acad. Sci.* **112**, 12249 (2015).
 - [8] J. S. Bullock and M. Boylan-Kolchin, *Annu. Rev. Astron. Astrophys.* **55**, 343 (2017).
 - [9] B. Moore, *Nature* **370**, 629 (1994).
 - [10] J. F. Navarro, C. S. Frenk, and S. D. M. White, *Astrophys. J.* **462**, 563 (1996).
 - [11] J. F. Navarro, A. Ludlow, V. Springel, J. Wang, M. Vogelsberger, S. D. M. White, A. Jenkins, C. S. Frenk, and A. Helmi, *MNRAS* **402**, 21 (2010).
 - [12] A. Saburova and A. D Popoloć, *MNRAS* **445**, 3512 (2014).
 - [13] B. Moore, S. Ghigna, F. Governato, G. Lake, T. Quinn, J. Stadel, and P. Tozzi, *Astrophys. J. Lett.* **524**, L19 (1999).
 - [14] A. Klypin, A. V. Kravtsov, O. Valenzuela, and F. Prada, *Astrophys. J.* **522**, 82 (1999).
 - [15] P. Agnes, I. F. M. Albuquerque, T. Alexander, A. K. Alton, G. R. Araujo, D. M. Asner, M. Ave, H. O. Back, B. Baldin, G. Batignani, et al., *Phys. Rev. Lett.* **121**, 081307 (2018).
 - [16] W. Hu, R. Barkana, and A. Gruzinov, *Phys. Rev. Lett.* **85**, 1158 (2000).
 - [17] J. Goodman, *New Astron.* **5**, 103 (2000).
 - [18] P. Mocz, L. Lancaster, A. Fialkov, F. Becerra, and P. H. Chavanis, *Phys. Rev. D* **97**, 083519 (2018).
 - [19] P. Mocz, A. Fialkov, M. Vogelsberger, F. Becerra, A. A. Amin, S. Bose, M. Boylan-Kolchin, P. H. Chavanis, L. Hernquist, L. Lancaster, F. Marinacci, V. H. Robles, and J. Zavala, *Phys. Rev. Lett.* **123**, 141301 (2019).
 - [20] L. Ferrarese and D. Merritt, *Astrophys. J. Lett.* **539**, L9 (2000).
 - [21] K. Gebhardt, R. Bender, G. Bower, A. Dressler, S. M. Faber, A. V. Filippenko, R. Green, C. Grillmair, L. C. Ho, J. Kormendy, T. D. Lauer, J. Magorrian, J. Pinkney, D. Richstone, and S. Tremaine, *Astrophys. J. Lett.* **539**, L13 (2000).
 - [22] R. M. Reddick, R. H. Wechsler, J. L. Tinker, and P. S. Behroozi, *Astrophys. J.* **771**, 30 (2013).
 - [23] J. Barranco, A. Bernal, J. C. Degollado, A. Diez-Tejedor, M. Megevand, M. Alcubierre, D. Núñez, and O. Sarbach, *Phys. Rev. Lett.* **109**, 081102 (2012).
 - [24] J. Barranco, A. Bernal, J. C. Degollado, A. Diez-Tejedor, M. Megevand, D. Núñez, and O. Sarbach, *Phys. Rev. D* **96**, 024049 (2017).
 - [25] A. A. Avilez, T. Bernal, L. E. Padilla, and T. Matos, *MNRAS* **477**, 3257 (2018).
 - [26] L. Hui, D. Kabat, X. Li, L. Santoni, and S. S. Wong, *MNRAS* **2019**, 2019 (2019).
 - [27] E. Y. Davies and P. Mocz, *MNRAS* **492**, 5721 (2020).
 - [28] P. Tod and I. M. Moroz, *Nonlinearity* **12**, 12 (1999).
 - [29] M. Smole, M. Micic, and N. Martinović, *MNRAS* **451**, 1964 (2015).
 - [30] J. Franklin, Y. Guo, K. C. Newton, and M. Schlosshauer, *Classical Quant Grav* **33**, 075002 (2016).
 - [31] P. J. Salzman, *Investigation of the time-dependent Schroedinger-Newton equation* (University of California, Davis, 2005).
 - [32] L. Hui, *Annu. Rev. Astron. Astrophys.* **59**, 247 (2021).
 - [33] L. Hui, J. P. Ostriker, S. Tremaine, and E. Witten, *Phys. Rev. D* **95**, 043541 (2017).
 - [34] H. Y. Schive, T. Chiueh, and T. Broadhurst, *Nature Physics* **10**, 496 (2014).
 - [35] H. Y. Schive, M. H. Liao, T. P. Woo, S. K. Wong, T. Chiueh, T. Broadhurst, and W. P. Hwang, *Phys. Rev. Lett.* **113**, 261302 (2014).